Desalination 404 (2017) 304–312

Contents lists available at ScienceDirect

Desalination

journal homepage: www.elsevier.com/locate/desal

Evaluation of thin film nanocomposite reverse osmosis membranes for long-term brackish water desalination performance

Pinar Cay-Durgun [a,b], Cailen McCloskey [a], John Konecny [a], Afsaneh Khosravi [a], Mary Laura Lind [a,b,*]

[a] School for Engineering of Matter, Transport and Energy, Arizona State University, Tempe, AZ 85287, USA
[b] Nanosystems Engineering Research Center for Nanotechnology-Enabled Water Treatment, Arizona State University, Tempe, AZ, 85287, USA

HIGHLIGHTS

- NaA type zeolite nanoparticles embedded in polyamide membranes *via* interfacial polymerization process.
- Hand-cast TFC and TFN membranes were tested for ~3000 h in a cross-flow testing system.
- TFN membranes demonstrated enhanced water-salt permselectivity compared to TFC membranes.
- TFN membranes exhibited desalination performance stability over long term application.

ARTICLE INFO

Article history:
Received 8 June 2016
Received in revised form 18 October 2016
Accepted 27 October 2016
Available online 23 November 2016

Keywords:
Thin film nanocomposite membrane
Reverse osmosis
Nanoparticles
Long-term performance
Desalination

ABSTRACT

Nanoparticle addition in the currently widely used thin film composite (TFC) membranes is a promising technology to advance separation performance and bring novel functionality in membrane desalination processes. These thin film nanocomposite (TFN) membranes boast many advantages over their TFC counterparts such as increased water flux without compromising salt rejection and bacterial resistance. However, the stability of TFN membranes is unknown in industrial, long-term applications. Via interfacial polymerization, we synthesized a series of polyamide TFC and TFN membranes with different nanoparticle content, 0 wt%, 0.15 wt%, 0.30 wt%, in the casting solutions. At the United States Bureau of Reclamation's Water Quality Improvement Center in Yuma, AZ, the membranes were tested for ~3000 h in a lab-scale testing system. We characterized the physico-chemical nature and morphology of the membranes before and after the testing. All membranes exhibited relatively stable long-term separation performances. At the highest zeolite loading tested, in comparison with the TFC membrane, water permeance increased from 3.7 ± 0.6 μm MPa^{-1} s^{-1} to 5.3 ± 0.5 μm MPa^{-1} s^{-1} and solute rejection slightly increased from 97.4 ± 0.3% to 97.9 ± 0.1%. In this study, TFN membranes exhibited long-term desalination stability and improved separation performance compared to TFC membranes.

1. Introduction

Reverse osmosis (RO) is a pressure-driven membrane process which is currently the most dominant technology for water desalination because of its relatively low energy consumption compared to non-membrane based desalination processes (e.g, thermal processes such as multi-stage flash and distillation) [1]. From the first cellulose acetate membranes to the current polyamide thin film composite (TFC) membranes, permeability increased from 1.4 μm MPa^{-1} s^{-1} to 5.5–8.3 μm MPa^{-1} s^{-1} for seawater and 8.3–13.9 μm MPa^{-1} s^{-1} for brackish water with very high rejections (>99%) of ionic solutes, such as sodium and chloride [2,3]. This technology widely uses the thin film composite (TFC) polyamide (PA) membrane which consists of an interfacially polymerized, ultrathin, crosslinked, aromatic PA layer onto microporous polysulfone supported by a non-woven polyester layer. The interfacial polymerization is a complex process involving the condensation reaction of an amine and an acid chloride at the interface of an aqueous and organic solution [4]. This dense PA structure is highly salt selective and the thinness of this layer (~100 nm) enables high water permeance in wide temperature and pH ranges [5,6]. Nevertheless, further performance improvement of polyamide TFC membranes in desalination applications is challenging because of two main factors. First, the "upper bound" permeability/selectivity trade-off observed in polymeric membranes for gas separations [7] also constrains the maximum performance of polymeric desalination membranes [8]. Second, polyamide membranes are susceptible to damage from biological fouling, scaling, and free chlorine (the most common disinfection agent in water treatment) [9,10]. Biofilms on the PA surface increase the resistance of the total membrane, resulting in flux decline and

* Corresponding author.
E-mail address: mllind@asu.edu (M.L. Lind).

http://dx.doi.org/10.1016/j.desal.2016.10.014
0011-9164/

ultimately in lower membrane performance and lifetime [10]. Some fouling and scaling may be minimized through appropriate cross-flow conditions within the RO membrane module to minimize issues with concentration polarization [11,12]. Although free chlorine is a low-cost and effective disinfection chemical for reducing biofilm layers, the PA structure degrades after continuous exposure to trace amounts of chlorine (at amounts three orders of magnitude lower than the effective chlorine present in disinfected water [13]). The PA degradation may result in increasing the water flux and the salt passage [6,13]. On the other hand, water permeance, solute rejection, and operational robustness of the membrane highly affect the energy consumption and operational costs of RO desalination processes [1,5]. Thus, there is a need to address these membrane challenges in desalination processes.

Coatings of porous metals, metal oxides, and zeolites are applied to mesoporous ceramic membranes or metallic membranes formed to develop mechanically enhanced and chemically durable membranes for water purification processes [5,14]. Compared to polymeric membranes, defect-free, versatile zeolitic membranes may enhance desalination performances, however, they have higher membrane production costs [14,15]. Moreover, because of the rigid structure, zeolitic membranes have lower permeation surface area density in a membrane module, which may cause an increase in operational costs [14,16]. These membranes are therefore rarely used for commercial desalination processes [5,15,16].

Mixed Matrix Membranes (MMMs) have emerged as an alternative to pure polymeric membranes or zeolitic membranes [17]. MMMs are composed of an inorganic filler phase dispersed through a continuous polymer phase. Ideally, the MMM retains the desirable characteristics of the individual components while obviating their individual disadvantages. MMMs have been studied extensively for gas separation applications [18,19]. For water separation applications, recent studies of nanoparticles embedded into the thin film polyamide structure during an interfacial polymerization process showed improved membrane performance [20]. In these advanced membranes for water treatement various nanofillers have been studied such as zeolite nanoparticles [21–29], carbon nanotubes [30–33], silica [34–36], silver [30], and metal oxides [37]. Superhydrophilic, nanosized Linde Type A (LTA) zeolites have demonstrated promising results in thin film nanocomposite (TFN) polyamide membranes for RO processes [21,22,24–26]. This zeolite consists of an aluminosilicate framework with a molecular formula of $Na_{12}[(AlO_2)_{12}(SiO_2)_{12}]\cdot 27H_2O$ (lowest possible silicon/aluminum ratio in LTA is 2). Because of this aluminum rich structure, LTA is a super-hydrophilic zeolite. However, it may not be stable under acidic environments [28] (dealumination may occur at low pH [38]). LTA (NaA type) has 3-dimensional narrow-pores with a diameter of 4.2 Å [39], which is suitable for selecting water, but excluding hydrated ions and small organic molecules [40,41]. The 3-dimensional structure of the LTA pores ensures access to the pore regardless of how the zeolite is oriented in the polymer (and is much simpler to embed in membrane structure compared to 1-dimensional structures such as carbon-nanotubes which require precise orientation to take advantage of the pore structure). Polyamide membranes with incorporated LTA nanoparticles are hydrophilic and have higher flux and similar rejection when compared with commercial membranes [21,22,24–26]. Furthermore, previous research on TFN membranes has demonstrated an increase in properties (smoother and more hydrophilic surfaces) that limit bacterial adhesion to membrane surfaces in short-term bacterial adhesion tests [26]. However, the performances of TFNs vary as a function of the type, size, and concentration of nanoparticles [21,22,24]. In addition, there may be some "non-ideal effects" [42] in MMMs such as particle aggregation at higher zeolite loadings [43] and void or rigidified polymer formation at the polymer/particle interface [42]. This may result in decreased performance of the membrane. In our publication analyzing the permeance of pure zeolite-4A molecular sieves and nanocomposite zeolite-4A/polymeric MMMs for water separations, we demonstrated that transport may occur both at the molecular sieve/polymer matrix interface and through the molecular sieves [44]. However Turgman-Cohen et al. performed a molecular dynamic simulation study on pressure-driven water transport through thin film membranes of LTA zeolite [45]. Based on this simulation result, they hypothesize that preferential flow may be around the zeolite particles not through the zeolite pores [45].

Reverse osmosis desalination applications are divided into two primary categories based on feed type: brackish water or sea water. Feed water salinity ranges determine the type. In 2010, Kurth et al. published the long-term performance of TFN membranes (with unknown types of inorganic particles) for seawater desalination [46]. However, to our best knowledge, no publications report the long-term performance and stability of TFN membranes for brackish water desalination. The differences in feed water characteristics such as foulants and salinity, in addition to the operating conditions such as pressure and temperature, cause the flux and rejection of the membranes to vary between brackish water and seawater desalination [47].

The objective of our research is to evaluate the long-term effectiveness of mixed matrix nanocomposite membranes for treating brackish water with reverse osmosis (RO) in an operating plant environment. The ultimate impact of this research is to increase the amount of available technology for reclaiming and purifying water supplies with reduced energy demands. This is the first report on long-term performance of TFN membranes with brackish feed waters.

2. Experimental methods

2.1. Materials

Chemicals used in this manuscript are referred to with the following nomenclature. We used a polysulfone coated non-woven polyester ultrafiltration membrane (PSf, NanoH_2O) as a support membrane. We prepared monomer solutions of meta-phenylene diamine (MPD, 99%, Sigma-Aldrich) in ultrapure deionized water (milli-Q water, Millipore), and trimesoyl chloride (TMC, 98%, Spectrum) in the organic solvent Isoparrafin-G (Isopar-G, Sigma-Aldrich), for the synthesis of the thin polyamide film. We used freeze dried powdered Linde type A zeolites (LTA, 4A, Na^+, NanoScape) with an ~100 nm mean particle size. The post-cure rinses consisted of solutions of sodium hypochlorite (NaOCl, reagent grade, Sigma-Aldrich) and sodium bisulfite ($NaHSO_3$, reagent grade, Sigma-Aldrich).

2.2. Membrane synthesis

Our casting procedure is based on previously published methods [21,22,25,26]. Thin film composite (TFC) membranes are pure polyamide membranes without nanoparticles. Thin film nanocomposite (TFN) membranes are similar polyamide membranes, with nanoparticles dispersed in the TMC-Isopar-G monomer solution.

First, we prepared the MPD in water and TMC in organic solvent monomer solutions separately. The solutions were magnetically stirred at 300 rpm for at least 3 h prior to use.

For the casting, a sheet of polysulfone coated polyester support membrane was taped on all sides onto a glass plate. Then, we soaked the support into 3.5 wt% MPD in milli-Q water monomer solution for 2 min, with the active side (PSf side) facing down in the solution and the back of the plate not submerged. After lifting the plate from the amine solution, to increase the uniformity of the membrane surface, we removed the excess solution from the surface with a rubber fingerprint ink roller. Then, we immediately placed the MPD coated membrane vertically into a monomer solution of 0.15 wt% TMC in isopar-G for the interfacial polymerization reaction. After 1 min, we removed the plate from the solution and held it vertically for 2 min. We cured the membrane through a series of post-treatment rinses. First, the membrane was placed into a water bath at ~95 °C with active side up for 2 min. Then, the membrane was removed from the glass plate and placed into 1.5 mL L^{-1} NaOCl in deionized water for 2 min. We believe

that NaOCl removes the unreacted MPD on the structure. Next, the membrane was placed into 1 g L^{-1} $NaHSO_3$ in deionized water for 30 s. We believe $NaHSO_3$ neutralizes the unreacted NaOCl, which protects the polyamide from degradation caused by the chlorine. Finally, the membrane was placed into a fresh water bath at ~95 °C with active side down for 2 min. The resulting membranes were placed into 1 L of milli-Q water in a light-proof Nalgene bottle until testing.

The only difference between the TFC and TFN membrane synthesis procedures is that we dispersed LTA zeolite nanoparticles in the TMC-isopar G solution with ultra-sonication at 20 °C for 30 min. We poured the sonicated solution into the membrane vertical solution holder immediately prior to the polymerization reaction.

For this work, we synthesized three types of polyamide/LTA zeolite thin film membranes, each with a different zeolite loading: 0 wt%, 0.15 wt%, 0.30 wt% of nanoparticles in the TMC-organic solution. The names of each membrane set are TFC, TFN 0.15, and TFN 0.30, respectively.

2.3. Long-term performance test

The operators at the United States Bureau of Reclamation Water Quality Improvement Center (WQIC) in Yuma, AZ tested the hand-cast membranes synthesized at ASU nearly continuously in a small-scale 9-cell cross-flow test unit, as depicted in Fig. 1, for approximately 3000 h with an applied hydraulic pressure of 200 psi. They placed nine different samples into the nine cell WQIC system (in which the cells are in series) in such a way that, for each zeolite loading, two samples were taken from the first membrane and one sample from the second membrane with the same nanoparticle loading. In total, three TFC, three TFN 0.15, and three TFN 0.30 membrane coupons were tested during the long-term performance test. The feed flow rate of the system was 1.5 gal min^{-1} and the effective membrane area tested for each cell was 18.37 cm^2. Prior to sending the membrane coupons to the WQIC for long term testing, we confirmed their defect-free nature through short term water flux and rejection measurements in a cross-flow laboratory-scale RO system at ASU.

At the WQIC, our membranes were tested with feed of controlled waters without pH adjustment. The WQIC operators measured flow rate, conductivity, temperature and pressure measurements every 12 h for both feed and permeate products. They also took the pH and free chlorine measurements of the feed. Additionally, once a week they analyzed the feed composition. Table 1 gives the key feed water parameters. The feed had a relatively narrow pH range, low chlorine concentration and dissolved salt content. The feed also had a low fouling character (total organic content <0.5 mg L^{-1}).

Table 1
Long-term performance test feed key parameters.

	Average	Range
pH	5.69	4.06–6.30
Free Chlorine (mg L^{-1})	0.048	0–0.585
Pressure (kPa)	1389	1340–2223
Temperature (°C)	29.8	20.4–39.1
Conductivity (μS cm^{-1})	734	529–1040

To evaluate the membrane performances, we obtained the salt water flux (J) [μm s^{-1}] from the flow rate divided by the membrane area. We calculated observed water permeance (A), often called the water permeability coefficient, by normalizing the flux by the applied pressure (ΔP) and the osmotic pressure ($\Delta\pi$) difference as $A = J/(\Delta P - \Delta\pi)$ [μm MPa^{-1} s^{-1}]. In addition, we calculated the observed rejection from $R = 1 - C_p/C_f$ where C_p and C_f [S cm^{-1}] were the conductivity of the permeate and the feed solution respectively. The salt permeance (B) was determined by $B = J(1 - R)/R$ [μm s^{-1}]. Finally, we calculated the water-salt permselectivity (A/B) by $A/B = R/(\Delta P - \Delta\pi)(1 - R)$ [MPa^{-1}]. In our calculations, to evaluate the membranes under the same conditions, we calculated the performances under observed condition and assumed no concentration polarization (for low salinity water testing under low pressure, the assumption may valid [48]).

2.4. Membrane characterization

We measured the contact angles of the membranes with de-ionized water sessile drop contact angle analysis (Easy Drop; Krűss) to evaluate surface hydrophilicity of all membranes. The drop volume of the water was 1 μL. The steady-state values of the angles on both sides of the drop were measured on air-dried samples. Twelve measurements were taken on each membrane sample. We removed the highest and the lowest values, and reported the average value and the standard deviation of the remaining measurements. We used attenuated total reflectance–Fourier transform infrared (ATR–FTIR, 6700 FTIR; Thermo Nicolet) with diamond crystal smart orbit to provide insight into the functionality of the thin film. We dried the membrane samples in a desiccator overnight prior to ATR-FTIR measurement. We used scanning electron microscopy (SEM, ESEM XL-30, Philips) to determine the surface morphology of the membranes at various magnifications. Dried membrane samples were sputter coated with Au—Pd prior to SEM analysis. SEM was performed at a 5–10 kV beam accelerating voltage. We used atomic force microscopy (AFM, Dimension 3000; Digital Instruments) to

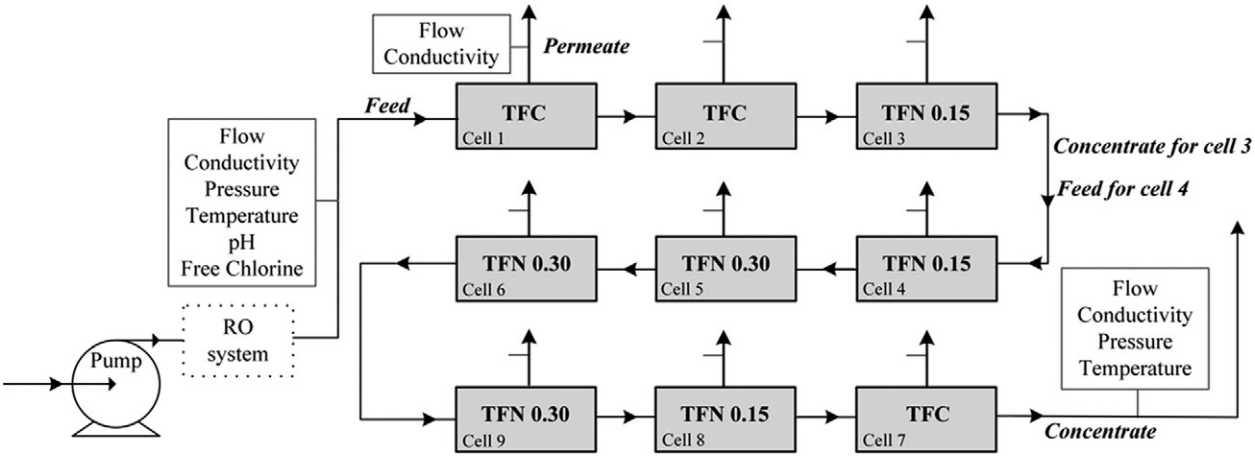

Fig. 1. The schematic of reverse osmosis test system in Water Quality Improvement Center at Yuma, AZ for evaluating hand-cast membranes' long-term separation performances. TFC, TFN 015, and TFN 0.30 represents the membrane type tested in the cell where thin film composite (TFC, as a control, without zeolite) and thin film nanocomposite (TFN 0.15 with 0.15 wt% zeolite, and TFN 0.30 with 0.30 wt% zeolite).

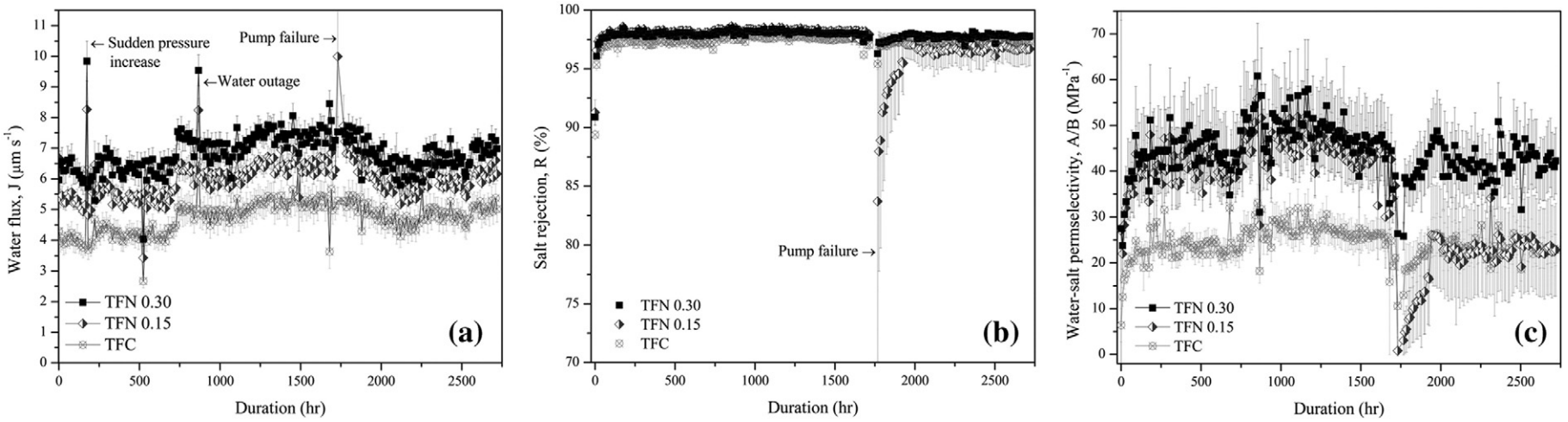

Fig. 2. Average measured performances of TFC, TFN 0.15, and TFN 0.30 membranes under 200 psi. (a) Water flux. (b) Salt rejection. (c) Water-salt permselectivity.

quantify roughness of the dried membranes at a fixed scanning rate of 1 Hz. The tip radius was 8–12 nm, the cantilever length was 215–235 μm with a spring constant of 3 N m^{-1}. For AFM analysis, three measurements were taken on each sample for 25 μm^2 scan area. We employed the tapping mode because polymers could be easily damaged by the tip. We reported the roughness in terms of the root-mean squared (RMS) roughness, the standard deviation of the averaged roughness, and surface area difference (SAD), the increase of the 3-D surface area over the 2-D surface area.

3. Results and discussion

3.1. Long term performance evaluation

The operators at the WQIC collected data from the system twice a day for 2760 h; they emailed the raw data to ASU where we analyzed it. Operating conditions such as pressure and temperature govern reverse osmosis performance. Pressure difference is the driving force for water flux, however the pressure difference does not have a large influence on salt passage. Consequently, separation performance is enhanced with increasing applied pressure. However, high applied pressure results in increased power consumption and operational costs. In our experiment, the system had overall stable pressure except on three occasions. There was a sudden pressure increase at 174 h into the test, a scheduled plant water supply outage at 996 h into the test and a pump failure at 1765 h into the test. Abrupt pressure changes might lead to possible membrane damage.

In addition, the temperature of the WQIC feed fluctuates throughout the day; there is an overall increase in daily temperature with time during the testing period. The measurements were taken twice daily at approximately the same times each day, and the temperature fluctuates (because the test started in May and ended in September). Therefore, the feed temperature increased as a result of the external weather during the long-term test. Feed viscosity, salt diffusivity and concentration polarization are largely dependent on temperature. Increases in temperature enhance the water and salt permeation through the membrane, thus, the flux performance increases and the salt rejection performance decreases [49,50].

In addition to pressure and temperature, feed composition also has an effect on the membrane performance. Conductivity (proportional to the concentration of total dissolved salts) and pH (concentration of hydronium ions) can be used to evaluate the feed composition effect on the long-term tests. However, conductivity and pH are functions of temperature [51,52]. Moreover, during the test, the feed composition also changed independently from the temperature. Therefore, we could not distinguish the actual individual contributions of composition, temperature, and pH on our tested membranes. But still we examined the flux response to the changed parameters in terms of stability. We concluded that the performance stabilities are similar for TFC and TFN membranes for brackish water desalination.

We averaged the performances of the samples for each membrane set, TFC, TFN 0.15, and TFN 0.30. Fig. 2 presents the averaged performance results (water flux Fig. 2a, salt rejection Fig. 2b, water-salt permselectivity Fig. 2c) and Table 2 exhibits all the averaged performance results (water flux, salt rejection, water permeance, salt permeance, water/salt permselectivity). The average brackish water permeance of the membranes with 0 wt%, 0.15 wt% and 0.30 wt% zeolite loadings were calculated as 3.7 ± 0.6, 4.7 ± 0.3 and 5.3 ± 0.5 μm MPa^{-1} s^{-1}, respectively. There is a 21% permeance increase for TFN 0.15 membranes compared to TFC membranes (with no zeolites). Moreover, the permeance improvement for TFN 0.30 membranes is 43% compared to the TFC membranes. These results show that water permeance increases with the zeolite loading, as expected. We obtained the maximum salt rejection for TFN 0.30 membranes of 97.9 ± 0.1%. We obtained similar salt rejection for TFC and TFN 0.15 membranes, 97.4 ± 0.3% and 97.2 ± 1.0% respectively.

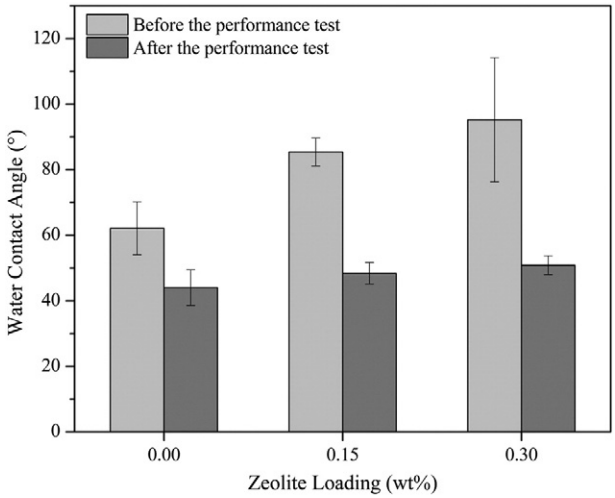

Fig. 3. Average pure water contact angle of the hand-cast TFC and TFN membranes before and after the long term performance test.

As can be seen in Fig. 2, the performance results indicate that all the membranes recovered their performance after the first abrupt pressure change (around 174 h) and the scheduled water outage (around 996 h). However, after the pump failure (at 1765 h), one of the TFN 0.15 membrane had a dramatic decrease in the salt rejection performance. After that, it took 3–4 days for the membrane to partially recover its pre-outage performance. After the recovery, its average salt rejection was recorded as 95.3 ± 0.4% compared to 98.2 ± 0.1% before the pump failure. Upon examination of the membrane surfaces after the end of the long-term test at the WQIC, we also observed color changes on the edges of active side surface of one of the three TFN 0.15 membranes. We did not observe such color changes on the other membranes. We hypothesize that there was damage to the membrane surface resulting from the abrupt pressure change created by the power failure, and that this damage influenced the salt rejection.

3.1. Membrane properties

We performed sessile drop contact angle analysis for all membranes before and after the performance test. Because of the presence of superhydrophilic nanoparticles, other researchers have found that thin film mixed matrix membranes show lower pure water contact angle than corresponding thin film polymer membranes [22,24,25]. Therefore, we expected to observe smaller contact angles with increasing zeolite content. However, as seen in Fig. 3, before the performance test, TFN

Table 2
Summary of the long-term separation performances.

Membrane set	LTA loading (wt%)	Water flux, J (μm s^{-1})	Salt rejection, R (%)	Water permeance, A (μm MPa^{-1} s^{-1})	Salt permeance, B (μm s^{-1})	Water-salt permselectivity, A/B (MPa^{-1})
TFC	0.00	4.8 ± 0.5	97.4 ± 0.3	3.7 ± 0.6	0.16 ± 0.01	24.2 ± 3.47
TFN 0.15	0.15	6.0 ± 0.6	97.2 ± 1.0	4.7 ± 0.3	0.21 ± 0.11	34.4 ± 7.36
TFN 0.30	0.30	6.8 ± 0.6	97.9 ± 0.1	5.3 ± 0.5	0.12 ± 0.02	44.2 ± 8.59

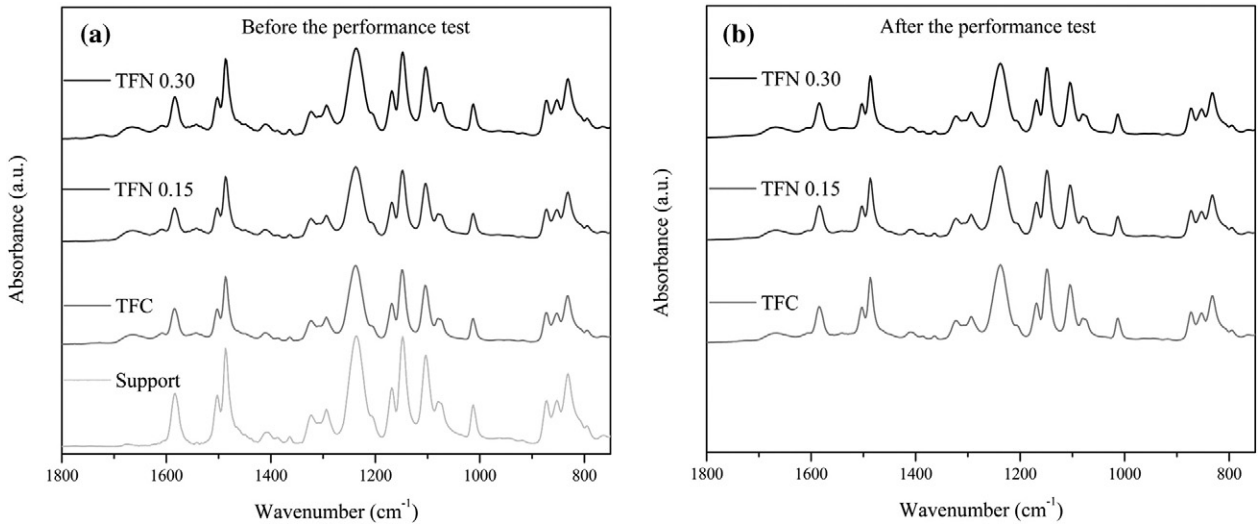

Fig. 4. Detailed ATR-FTIR spectra of hand-cast TFC and TFN membranes from 1800 to 750 cm^{-1} (a) as synthesized, (b) after the long-term performance test at the WQIC.

membranes demonstrated higher average water contact angle results than corresponding TFC membranes. We hypothesize this unexpected result is partially attributable to the presence of zeolite aggregation which yields a rough non-uniform surface. This hypothesis may also explain the decrease in contact angle values after the performance test. Previously, we have observed aggregation of LTA zeolite nanoparticles in polyamide membranes. Mechanical compaction during the performance test may release any loosely bonded zeolite clumps from the membrane surface, which could result in the observed decrease in the contact angle values of TFN membranes compare the values of before performance test.

Fig. 4 shows the detailed ATR-FTIR spectra of TFC and TFN membranes in the range from 1800 cm^{-1} to 750 cm^{-1} before and after the performance test. The broad peak at 1050–950 cm^{-1} is characteristic of Si—O and Al—O functionality in LTA zeolites [27]. In Fig. 4a the increase of the peak at ~1010 cm^{-1} for 0.30 wt% zeolite loading membranes may confirm the presence of zeolite in our mixed-matrix nanocomposites films. In addition, to obtain insight into chemical functionality and extent of crosslinking in our TFC and TFN membranes, we focused on the peaks at ~1540 cm^{-1}, at ~1609 cm^{-1}, ~1663 cm^{-1}, and at ~1734 cm^{-1}, which correspond to the C—N stretch of amide II band, the aromatic amide band, the amide I band, and the C═O carboxylic acid band in the cast TFC and TFN membranes [25,27]. All of these peaks are characteristic to polyamide. Based on the chemical structure of polyamide formation from MPD and TMC monomers, the linear polymer structure has more carboxylic acid functionality (ATR-FITR peak ~1734 cm^{-1}) [25]. Previously, Lind et al. observed that TFN RO membranes exhibit an increase in absorbance of the characteristic peaks at 1734 cm^{-1} (corresponding to the C═O carboxylic functionality) compared to TFC RO membranes. [25] Additionally, Lind et al. measured extent of crosslinking of these membranes using X-ray photoelectron spectroscopy and found less cross-linking in the TFN membranes compared to the TFC membranes. Ma et al. also observed that TFN forward osmosis membranes exhibit an increase in absorbance of the characteristic peaks at 1734 cm^{-1} as compared to TFC membranes [27]. These results combined with the knowledge that the linear structure of the polyamide formed from MPD and TMC has more carboxylic acid functionality are in line with our observation: that TFN 0.30 membranes exhibit more intense peaks at 1734 cm^{-1} than the TFC membranes, thus semi-quantitatively indicating a less cross-linked structure. In addition, the peak at ~1540 cm^{-1} appears to begin splitting with addition of zeolite. It means that our TFN membranes have fewer C—N bonds, which corresponds to a less crosslinked polymer structure [25]. In Fig. 4b, the ATR-FTIR spectra for all membranes are almost identical to each other after the long-term performance test. The peaks are still characteristic to polyamide, but are of lower intensity. Physical compaction, which decreased the thickness of the films, may explain the weakened intensity of the characteristic PA peaks.

Fig. 5 presents SEM images of the polyamide/zeolite surface for all TFC and TFN membranes. We observed that the surface of hand cast polyamide (MPD/TMC) and zeolite/polyamide membranes are similar to characteristic polyamide thin film composite membranes with “hill and valley” or “ridge and valley” structures [22,27,53]. We did not observe a noticeable polymer structure change with increased zeolite loading. However, we encountered zeolite clumps on the surface of TFN membranes, as displayed in Fig. 6. This zeolite aggregation may impact the polymer structure and membrane performance. Dong et al. proposed a surface modification method in a published report to

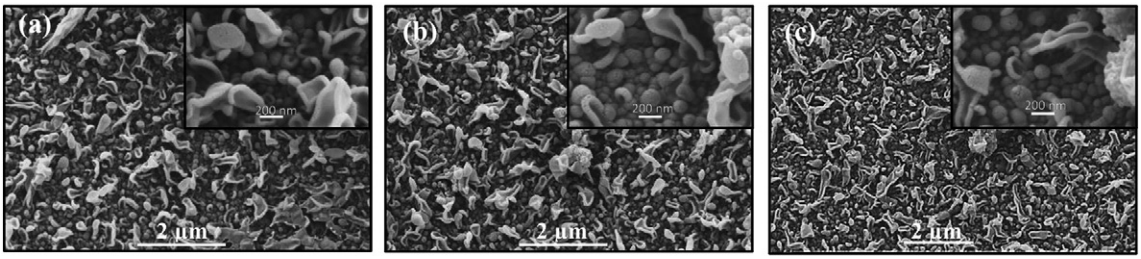

Fig. 5. SEM images of TFC and TFN membranes nanoparticle loadings are (a) 0.0 wt%, (b) 0.15 wt%, (c) 0.30 wt%.

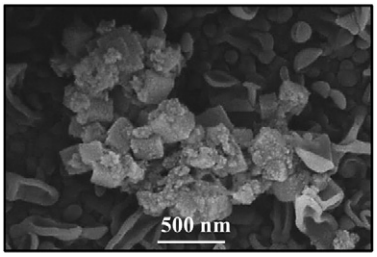

Fig. 6. SEM image for zeolite aggregation on TFN 0.30 membrane prior to the test.

overcome the zeolite aggregation problem [24]. In the future, applying this procedure may minimize particle aggregation in thin film mixed matrix membranes.

We examined the surface morphologies of the WQIC tested membranes with SEM after completion of the long-term testing. The representative images are in Fig. 7. We did not observe a significant polyamide structure change. Fouling leads to decreased membrane permeance and decreased salt rejection [10]. Because we did not have significant membrane performance impairment and the feed had low organic content, we expected a negligible fouling rate in this experiment. Indeed, we noticed minimal deposition on and color change of the membrane surface. Visually, the higher zeolite loaded TFN membranes have the cleanest surfaces.

Fig. 8 presents atomic force microscopy analysis. We quantified surface roughness of all membranes with two parameters: root mean square roughness (RMS) and surface area difference (SAD). RMS represents the standard deviation of the height values within a scan area. SAD provides the percentage difference between the three dimensional surface area over the two dimensional surface area. Larger RMS and SAD values correspond to rougher membranes [25]. Before the performance test, while TFN 0.15 membranes had smallest RMS values, TFN 0.30 membranes have significantly higher RMS value than TFC membranes. For TFN 0.30 membranes, due to structural difference and/or zeolite aggregation, we might have higher roughness difference. Compaction of the membrane coupled with washing off of zeolite aggregates could account for the observed reduction in RMS value after the performance test for the TFN 0.30 membranes. In addition, we observed increased roughness for TFC and TFN 0.15 membranes after the performance test compared to untested membranes. Surface deposition of potential foulants or scalants might explain this behavior. Generally, others have observed that TFN membranes were rougher with more surface area compared to TFC membranes [25]. According to our SAD results, prior to the performance test, our TFN membranes were rougher with increased zeolite loading. This result correlated with our contact angle as well as water permeance results. However, after the performance test, the high zeolite loaded TFN membranes SAD results shows that they become smoother during the performance test. We hypothesized that the aggregated zeolites might be washed off creating smoother membrane surfaces. Table 3 summarizes the membrane physical property characterization for the membranes before and after the long-term performance test.

4. Conclusions

We evaluated the long-term performance of our hand-cast thin film composite and thin film nanocomposite membranes. Except for a scheduled plant water supply outage and a pump failure, our

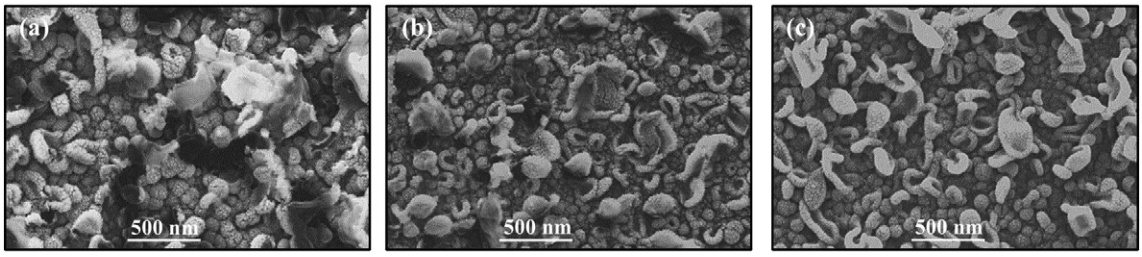

Fig. 7. SEM images for surface morphology of the membranes after the long-term performance test at the WQIC. (a) TFC membrane, (b) TFN 0.15 membrane, (c) TFN 0.30 membrane.

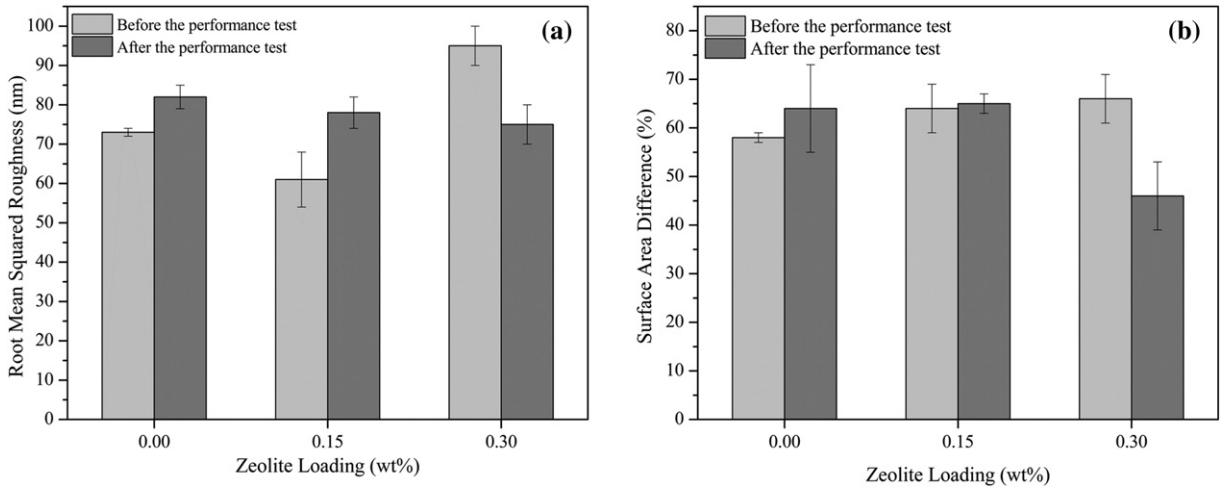

Fig. 8. Average surface property of TFC and TFN membranes before and after the long-term performance test. (a) Root mean squared roughness, (b) Surface area difference.

Table 3
Summary of membrane physical properties before and after the performance test.

Membrane set	LTA loading (wt%)	Contact angle* (°)	Contact angle** (°)	RMS* (nm)	RMS** (nm)	SAD* (%)	SAD** (%)
TFC	0.00	62.1 ± 8.1	44.0 ± 5.4	72.9 ± 1.1	81.6 ± 2.6	58.3 ± 1.1	64.3 ± 8.6
TFN 0.15	0.15	85.4 ± 4.3	48.4 ± 3.2	60.9 ± 6.5	77.6 ± 3.6	64.2 ± 5.1	65.0 ± 1.9
TFN 0.30	0.30	95.2 ± 18.9	50.8 ± 2.8	94.7 ± 5.4	74.6 ± 5.0	66.0 ± 5.1	46.1 ± 7.3

* Before long-term performance test.
** After long-term performance test.

membranes were tested for approximately 3000 h in an operating plant environment. All TFN membranes demonstrated higher salt water flux than the TFC membranes while maintaining similar average salt rejection. The TFN membranes with 0.15 wt% LTA content had a 1.3 times higher water permeance than the TFC membranes and those with 0.30 wt% LTA content had a 1.4 times higher water permeance than the TFC membranes. In addition, TFN membranes had higher salt selectivity than the TFC membranes (TFN 0.15 and TFN 0.30 membranes exhibited 1.4 and 1.8 times higher permselectivities than TFC membranes). The long-term performance data demonstrate that increases in zeolite loading enhanced long-term separation performance (both water permeance and salt selectivity) for brackish water reverse osmosis desalination.

Our results show that thin film nanocomposite membranes had stable long-term flux and rejection performance in comparison to thin film composite membranes. However, we did not evaluate the membranes under high fouling and extreme pH conditions. In addition the membranes did not experience cleaning or chemical treatments. Thus, there is a need for continued research into their tolerance to harsh fouling and chemical environments to validate their possible contribution to reduce the energy consumption for brackish water desalination.

Acknowledgements

This work was supported by a United States Department of The Interior, Bureau of Reclamation – cooperative agreement #R13AC3400 and the Ira A. Fulton Schools of Engineering at Arizona State University. Article preparation was supported by the NSF Nanosystems Engineering Research Center for Nanotechnology-Enabled Water Treatment (ERC-1449500).

We are very grateful to Dr. Thaddeus Graczky from Northern Arizona University, Angela Adams of the USBR Richard Bash, Dr. Charles D. Moody and WQIC operations personnel for their collaboration. We would like to acknowledge lab manager Fred Pena at ASU for his extensive help building custom made reverse osmosis testing system. We gratefully acknowledge the use of characterization facilities at the LeRoy Erying Center for Solid State Science and the Bio-Design Institute at Arizona State University.

References

[1] D. Li, H.T. Wang, Recent developments in reverse osmosis desalination membranes, J. Mater. Chem. 20 (2010) 4551–4566.
[2] T. Hodgson, Selective properties of cellulose acetate membranes towards ions in aqueous solutions, Desalination 8 (1970) 99–138.
[3] J.R. Werber, A. Deshmukh, M. Elimelech, The critical need for increased selectivity, not increased water permeability, for desalination membranes, Environ. Sci. Technol. Lett. 3 (2016) 112–120.
[4] B. Khorshidi, T. Thundat, B.A. Fleck, M. Sadrzadeh, A novel approach toward fabrication of high performance thin film composite polyamide membranes, Sci. Rep. 6 (2016) 22069.
[5] M.M. Pendergast, E.M.V. Hoek, A review of water treatment membrane nanotechnologies, Energy Environ. Sci. 4 (2011) 1946–1971.
[6] G.M.L., H.S. Geise, D.J. Miller, B.D. Freeman, J.E. Mcgrath, D.R. Paul, Water purification by membranes: the role of polymer science, J. Polym. Sci. Polym. Phys. 48 (2010) 1685–1718.
[7] L.M. Robeson, Correlation of separation factor versus permeability for polymeric membranes, J. Membr. Sci. 62 (1991) 165–185.
[8] G.M. Geise, H.B. Park, A.C. Sagle, B.D. Freeman, J.E. McGrath, Water permeability and water/salt selectivity tradeoff in polymers for desalination, J. Membr. Sci. 369 (2011) 130–138.
[9] J. Glater, S.K. Hong, M. Elimelech, The search for a chlorine-resistant reverse-osmosis membrane, Desalination 95 (1994) 325–345.
[10] A. Matin, Z. Khan, S.M.J. Zaidi, M.C. Boyce, Biofouling in reverse osmosis membranes for seawater desalination: phenomena and prevention, Desalination 281 (2011) 1–16.
[11] M. Goosen, S. Sablani, H. Al-Hinai, S. Al-Obeidani, R. Al-Belushi, D. Jackson, Fouling of reverse osmosis and ultrafiltration membranes: a critical review, Sep. Sci. Technol. 39 (2005) 2261–2297.
[12] E.M. Hoek, A.S. Kim, M. Elimelech, Influence of crossflow membrane filter geometry and shear rate on colloidal fouling in reverse osmosis and nanofiltration separations, Environ. Eng. Sci. 19 (2002) 357–372.
[13] H.B. Park, B.D. Freeman, Z.B. Zhang, M. Sankir, J.E. McGrath, Highly chlorine-tolerant polymers for desalination, Angew. Chem. 120 (2008) 6108–6113.
[14] A. Rodríguez-Calvo, G. Silva-Castro, F. Osorio, J. González-López, C. Calvo, Novel membrane materials for reverse osmosis desalination, Hydrol. Current. Res. 5 (2014) 2.
[15] S. Daer, J. Kharraz, A. Giwa, S.W. Hasan, Recent applications of nanomaterials in water desalination: a critical review and future opportunities, Desalination 367 (2015) 37–48.
[16] K.P. Lee, T.C. Arnot, D. Mattia, A review of reverse osmosis membrane materials for desalination—development to date and future potential, J. Membr. Sci. 370 (2011) 1–22.
[17] C.M. Zimmerman, A. Singh, W.J. Koros, Tailoring mixed matrix composite membranes for gas separations, J. Membr. Sci. 137 (1997) 145–154.
[18] G.X.L. Dong, H. Y., V.K. Chen, Challenges and opportunities for mixed-matrix membranes for gas separation, J. Mater. Chem. A 1 (2013) 4610–4630.
[19] T.-S. Chung, L.Y. Jiang, Y. Li, S. Kulprathipanja, Mixed matrix membranes (MMMs) comprising organic polymers with dispersed inorganic fillers for gas separation, Prog. Polym. Sci. 32 (2007) 483–507.
[20] W. Lau, S. Gray, T. Matsuura, D. Emadzadeh, J.P. Chen, A. Ismail, A review on polyamide thin film nanocomposite (TFN) membranes: history, applications, challenges and approaches, Water Res. 80 (2015) 306–324.
[21] M.L. Lind, A.K. Ghosh, A. Jawor, X.F. Huang, W. Hou, Y. Yang, E.M.V. Hoek, Influence of zeolite crystal size on zeolite-polyamide thin film nanocomposite membranes, Langmuir 25 (2009) 10139–10145.
[22] B.H. Jeong, E.M.V. Hoek, Y.S. Yan, A. Subramani, X.F. Huang, G. Hurwitz, A.K. Ghosh, A. Jawor, Interfacial polymerization of thin film nanocomposites: a new concept for reverse osmosis membranes, J. Membr. Sci. 294 (2007) 1–7.
[23] M. Fathizadeh, A. Aroujalian, A. Raisi, Effect of added NaX nano-zeolite into polyamide as a top thin layer of membrane on water flux and salt rejection in a reverse osmosis process, J. Membr. Sci. 375 (2011) 88–95.
[24] H. Dong, X.Y. Qu, L. Zhang, L.H. Cheng, H.L. Chen, C.J. Gao, Preparation and characterization of surface-modified zeolite-polyamide thin film nanocomposite membranes for desalination, Desalin. Water Treat. 34 (2011) 6–12.
[25] M.L. Lind, D.E. Suk, T.V. Nguyen, E.M.V. Hoek, Tailoring the structure of thin film nanocomposite membranes to achieve seawater RD membrane performance, Environ. Sci. Technol. 44 (2010) 8230–8235.
[26] M.L. Lind, B.H. Jeong, A. Subramani, X.F. Huang, E.M.V. Hoek, Effect of mobile cation on zeolite-polyamide thin film nanocomposite membranes, J. Mater. Res. 24 (2009) 1624–1631.
[27] N. Ma, J. Wei, R.H. Liao, C.Y.Y. Tang, Zeolite-polyamide thin film nanocomposite membranes: towards enhanced performance for forward osmosis, J. Membr. Sci. 405 (2012) 149–157.
[28] H. Huang, X. Qu, X. Ji, X. Gao, L. Zhang, H. Chen, L. Hou, Acid and multivalent ion resistance of thin film nanocomposite RO membranes loaded with silicalite-1 nanozeolites, J. Mater. Chem. A 1 (2013) 11343–11349.
[29] H. Huang, X. Qu, H. Dong, L. Zhang, H. Chen, Role of NaA zeolites in the interfacial polymerization process towards a polyamide nanocomposite reverse osmosis membrane, RSC Adv. 3 (2013) 8203–8207.
[30] E.-S. Kim, G. Hwang, M.G. El-Din, Y. Liu, Development of nanosilver and multi-walled carbon nanotubes thin-film nanocomposite membrane for enhanced water treatment, J. Membr. Sci. 394 (2012) 37–48.
[31] J. Park, W. Choi, S.H. Kim, B.H. Chun, J. Bang, K.B. Lee, Enhancement of chlorine resistance in carbon nanotube based nanocomposite reverse osmosis membranes, Desalin. Water Treat. 15 (2010) 198–204.
[32] S. Roy, S.A. Ntim, S. Mitra, K.K. Sirkar, Facile fabrication of superior nanofiltration membranes from interfacially polymerized CNT-polymer composites, J. Membr. Sci. 375 (2011) 81–87.
[33] W.-F. Chan, H.-y. Chen, A. Surapathi, M.G. Taylor, X. Shao, E. Marand, J.K. Johnson, Zwitterion functionalized carbon nanotube/polyamide nanocomposite membranes for water desalination, ACS Nano 7 (2013) 5308–5319.

[34] J. Yin, E.-S. Kim, J. Yang, B. Deng, Fabrication of a novel thin-film nanocomposite (TFN) membrane containing MCM-41 silica nanoparticles (NPs) for water purification, J. Membr. Sci. 423 (2012) 238–246.
[35] G.L. Jadav, P.S. Singh, Synthesis of novel silica-polyamide nanocomposite membrane with enhanced properties, J. Membr. Sci. 328 (2009) 257–267.
[36] M. Bao, G. Zhu, L. Wang, M. Wang, C. Gao, Preparation of monodispersed spherical mesoporous nanosilica–polyamide thin film composite reverse osmosis membranes via interfacial polymerization, Desalination 309 (2013) 261–266.
[37] C. Kong, T. Kamada, T. Shintani, M. Kanezashi, T. Yoshioka, T. Tsuru, Enhanced performance of inorganic-polyamide nanocomposite membranes prepared by metal-alkoxide-assisted interfacial polymerization, J. Membr. Sci. 366 (2011) 382–388.
[38] H.L. Jamieson, H. Yin, A. Waller, A. Khosravi, M.L. Lind, Impact of acids on the structure and composition of Linde Type A zeolites for use in reverse osmosis membranes for recovery of urine-containing wastewaters, Microporous Mesoporous Mater. 201 (2015) 50–60.
[39] D. Breck, W. Eversole, R. Milton, T. Reed, T. Thomas, Crystalline zeolites. I. The properties of a new synthetic zeolite, type A, J. Am. Chem. Soc. 78 (1956) 5963–5972.
[40] B. Tansel, J. Sager, T. Rector, J. Garland, R.F. Strayer, L. Levine, M. Roberts, M. Hummerick, J. Bauer, Significance of hydrated radius and hydration shells on ionic permeability during nanofiltration in dead end and cross flow modes, Sep. Purif. Technol. 51 (2006) 40–47.
[41] B. Van der Bruggen, J. Schaep, D. Wilms, C. Vandecasteele, Influence of molecular size, polarity and charge on the retention of organic molecules by nanofiltration, J. Membr. Sci. 156 (1999) 29–41.
[42] T.T. Moore, W.J. Koros, Non-ideal effects in organic–inorganic materials for gas separation membranes, J. Mol. Struct. 739 (2005) 87–98.
[43] D.Q. Vu, W.J. Koros, S.J. Miller, Mixed matrix membranes using carbon molecular sieves: I. Preparation and experimental results, J. Membr. Sci. 211 (2003) 311–334.
[44] P. Cay-Durgun, S.G. Fink, A. Shabilla, H. Yin, K.A. Sasaki, M.L. Lind, Analysis of the water permeability of Linde Type A zeolites in reverse osmosis, Sep. Sci. Technol. 49 (2014) 2824–2833.
[45] S. Turgman-Cohen, J.C. Araque, E.M. Hoek, F.A. Escobedo, Molecular dynamics of equilibrium and pressure-driven transport properties of water through LTA-type zeolites, Langmuir 29 (2013) 12389–12399.
[46] C.J. Kurth, R.L. Burk, J. Green, Improving seawater desalination with nanocomposite membranes, IDA J. Desalin. Water Reuse 2 (2010) 26–31.
[47] L.F. Greenlee, D.B. Fawler, B.D. Freeman, B. Marrot, P. Moulin, Reverse osmosis desalination: water sources, technology, and today's challenges, Water Res. 43 (2009) 2317–2348.
[48] L. Song, S. Yu, Concentration polarization in cross-flow reverse osmosis, American Institute of Chemical Engineers, AIChE J 45 (1999) 921.
[49] X. Jin, A. Jawor, S. Kim, E. Hoek, Effects of feed water temperature on separation performance and organic fouling of brackish water RO membranes, Desalination 239 (2009) 346–359.
[50] A. Jawor, E. Hoek, Effects of feed water temperature on inorganic fouling of brackish water RO membranes, Desalination 235 (2009) 44–57.
[51] J.J. Barron, C. Ashton, The Effect of Temperature on Conductivity Measurement, TSP-07, Issue 3, Technical Article of Reagent Diagnostics Ltd, 2007.
[52] J.J. Barron, C. Ashton, L. Geary, The Effects of Temperature on pH Measurement, TSP-01, Issue 2, Technical Article of Reagent Diagnostics Ltd, 2005.
[53] S.Y. Kwak, S.G. Jung, Y.S. Yoon, D.W. Ihm, Details of surface features in aromatic polyamide reverse osmosis membranes characterized by scanning electron and atomic force microscopy, J. Polym. Sci. Polym. Phys. 37 (1999) 1429–1440.